IOPscience iopscience.iop.org

Home Search Collections Journals About Contact us My IOPscience

Contribution of numerical simulation to silicon carbide bulk growth and epitaxy

This article has been downloaded from IOPscience. Please scroll down to see the full text article.

2004 J. Phys.: Condens. Matter 16 S1579

(http://iopscience.iop.org/0953-8984/16/17/009)

View the table of contents for this issue, or go to the journal homepage for more

Download details:
IP Address: 129.252.86.83
The article was downloaded on 27/05/2010 at 14:30

Please note that terms and conditions apply.

INSTITUTE OF PHYSICS PUBLISHING JOURNAL OF PHYSICS: CONDENSED MATTER

J. Phys.: Condens. Matter **16** (2004) S1579–S1595 PII: S0953-8984(04)65091-0

Contribution of numerical simulation to silicon carbide bulk growth and epitaxy

Jérôme Meziere[1,2], Michel Pons[1,4], Léa Di Cioccio[2], Elisabeth Blanquet[1], Pierre Ferret[2], Jean-Marc Dedulle[3], Francis Baillet[1], Etienne Pernot[3], Michaïl Anikin[3], Roland Madar[3] and Thierry Billon[2]

[1] LTPCM-INPG-CNRS, 1130 rue de la Piscine, BP 75, 38402 Saint Martin D'Hères, France
[2] CEA/DRT/LETI-CEA, 38054 Grenoble Cedex 9, France
[3] LMGP-INPG-CNRS, BP 46, 38402 Saint Martin D'Hères, France

E-mail: michel.pons@ltpcm.inpg.fr

Received 20 June 2003, accepted for publication 26 June 2003
Published 16 April 2004
Online at stacks.iop.org/JPhysCM/16/S1579
DOI: 10.1088/0953-8984/16/17/009

Abstract
High temperature epitaxial processes for SiC bulk and thin films by physical vapour transport and chemical vapour deposition are reviewed from an academic point of view using heat and mass transfer modelling and simulation. The objective is to show that this modelling approach could provide information on fabrication and characterization for the improvement of the knowledge of the growth history. Recent results of our integrated research programme on SiC, taking into account the fabrication, process modelling and characterization, will be presented.

(Some figures in this article are in colour only in the electronic version)

1. Introduction

Although silicon technology will dominate microelectronics for the foreseeable future, several important applications are limited by the fundamental material properties. Wide bandgap materials such as silicon carbide and III-nitrides have properties which make them attractive for high-power, high-frequency, high-temperature devices [1, 2]. The increasing interest in SiC is related to the availability of commercial substrates of ever-increasing diameter and quality [3] followed by the development of epitaxial growth techniques [4]. For instance, one of the main obstacles to reaching a larger-scale production of SiC devices is controlling the residual defects in the material and understanding how they affect device behaviour [5].

Physical vapour transport (PVT) via seeded sublimation, at temperatures above 2300 K, is the most common technique for the fabrication of 4H- and 6H-SiC boules with a growth

[4] Author to whom any correspondence should be addressed.

rate of about 0.5 mm h^{-1}. Recently, a high temperature chemical vapour deposition process (HTCVD) has proved its efficiency in processing large and long semi-insulating SiC boules [6]. The growth technique will be presented first, highlighting technological, physicochemical and process problems. Selected results of heat and mass transfer modelling and simulation will be associated with our experimental and characterization results to point out key growth parameters.

High quality homoepitaxial growth (3–10 μm h^{-1}) at around 1800–1900 K is generally achieved on off-axis SiC(0001) wafers, owing to the concept of step-controlled epitaxy (see in [4]) by chemical vapour deposition (CVD). Horizontal [7] and vertical cold wall [8–10], chimney [11], horizontal hot wall [12–16] and planetary reactors [17] can be used. More recently, chimney-type reactors working at high temperature (>2000 K) with hot walls were developed to increase the growth rate to 25–100 μm h^{-1} [11, 18, 19]. SiH_4 and C_3H_8 are generally used as precursors and H_2 as the carrier gas. N_2 and trimethylaluminium (TMA) or B_2H_6 precursors are used for n-type doping and for p-type doping, respectively. The challenges for these high temperature CVD processes are first to control the temperature and the concentration fields and second to understand and improve large-scale area deposition and doping uniformity. Recent results on the macroscopic modelling and simulation of the growth process in a hot wall reactor will be presented to highlight the combined effects of materials science and process engineering.

Section 2 will briefly develop the basis of the modelling. Section 3 will be concerned with calculations of the growth history of SiC bulk single crystals by PVT. Specific requirements for the modelling will be highlighted and selected results will demonstrate the potential of this approach in the field of crystal growth from the vapour phase. In section 4 the same modelling concepts will be applied to the CVD process of thin SiC films and their doping control. We will see that, although the relevant physical laws are well established, the modelling and the simulation, i.e. the tentative quantification of the macroscopic growth, needs further research effort in kinetic phenomena, but does give trends for experiments.

2. Modelling and simulation

The successful modelling of PVT and CVD reactors requires a combination of a number of different scientific areas in a multidisciplinary approach. The fundamentals of state-of-the-art models are formed by transport phenomena models consisting of a set of partial differential equations with appropriate boundary conditions describing the gas flow, the transport of energy and species and the production/destruction of species due to chemical reactions at the macroscopic scale. The model describes the motion of a mixture of ideal gases at high temperature and relatively low velocities. Such models are well developed and supported by various software packages. The model must be complemented by different submodels such as

(1) chemistry models describing the homogeneous and heterogeneous reaction mechanisms and thermodynamics and kinetics databases;
(2) a kinetic theory model for the description of transport properties of the gas mixture;
(3) a conjugate heat transfer model including the radiative, conductive and convective heat exchange between the heating source, susceptor, seed, wafer, reactor walls and surroundings.

Apart from gas and solid materials properties databases, inputs to the model include the description of the reactor geometry and process conditions. The results of the simulation at the reactor scale are growth rate and uniformity, film composition and dopant incorporation.

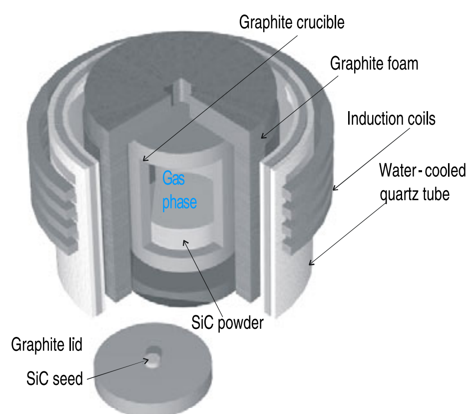

Figure 1. Schematic representation of the reactor and graphite lid.

3. Modelling and simulation of bulk growth

3.1. Introduction—specific needs

6H and 4H crystals are generally grown by the modified Lely method (figure 1). A common experimental set-up includes RF heating and a graphite crucible. The crucible is wrapped in graphite foam for thermal insulation and the whole assembly is placed inside a water-cooled quartz reactor. The growth temperature (measured on the top of the graphite lid) is about 2400 K and the argon pressure is in the range 0.2–1.5 kPa. The distance between the source and seed is in the range 10–20 mm. Under these experimental conditions 4H and 6H single crystals with a thickness of about 10 mm can be fabricated [20]. The growth rate is about 0.5 mm h^{-1}. Large-scale methods of characterization [21] and special techniques of polishing [22] play an important role in the development of the process and in its reproducibility.

In the course of the development of bulk growth processes, increased attention was paid to the crucible design and optimization of the thermal and concentration profiles in the growth cavity [23–38]. There is no way to control the behaviour of individual species and therefore the growth process can only be influenced through macroscopic mechanisms, such as thermal environment, mass transport and chemical reactions. These mechanisms are highly interdependent. A useful model should be able to predict quantitatively how these phenomena influence the crystal growth process. The results of modelling are usually twofold. Firstly, it gives an insight into what is actually happening in the system and, secondly, it helps in evaluating new systems without the need for actually building them.

In our group, for two-dimensional axisymmetric geometries, a software package has been initially built from commercial and in-house software packages [24, 25]. The available thermal, electrical and chemical databases are also inserted. Other software packages like CFDACE[5] or Virtual Reactor[6] [34] are available for this specific problem and can be easily used.

Thermodynamic modelling. The thermodynamic calculations were carried out by minimization of the total free energy of the Si–C–Ar system in the temperature range 2300–

[5] CFDACE is a product of CFD Research Corporation, 215 Wyan Drive, Huntsville, AL 35805, USA, http://www.cfdrc.com
[6] Virtual Reactor and Global Heat Transfer are products of Soft Impact, PO Box 33, Engelsa Prospekt 27, 194156, Saint-Petersburg, Russia, http://www.softimpact.ru

3000 K. A self-consistent set of data was generated for the gaseous molecules from a literature review, measurements, and heat capacity and entropy calculations using recent results on molecular structures, vibrational frequencies and electronic spectra. Nine gaseous species in addition to argon (Si_1, Si_2, Si_3, C_1, C_2, C_3, SiC, Si_2C, SiC_2) and three condensed phases (SiC, Si and C graphite) were considered [24, 37, 38]. Calculations show that only three species are of importance: Si_1, Si_2C, SiC_2.

Gas and surface chemistry. A comprehensive capability must be available to simulate multi-step gas and surface chemistry. Large sets of multi-step reactions or thermodynamic equilibrium must be handled in the code. The surface chemistry is treated by doing a complete reaction–diffusion balance at the surface to obtain the surface concentration of species. The heat release from the gas/surface reactions is included in the model.

The use of local thermodynamic equilibrium (LTE) assumes infinite length or timescale. We have checked that mass transport computations linked with LTE can give the correct trends in the crystal shape and on the influence of pressure, but the absolute growth rate found is too high. High temperature spectrometry (2000–2300 K) was used to evaluate sublimation coefficients. It is clear that the chemical system does not reach thermodynamic equilibrium. One order of magnitude difference has been recorded between equilibrium partial pressure and measured pressure. These data are now included in the models to compute the growth rates and crystal shapes [37, 38].

Induction heating and temperature distribution. Electromagnetodynamics must be coupled with heat transfer, especially radiative heat transfer within the growth cavity. The radiation model is tightly coupled to the fluid transport, conjugate heat transfer and chemistry models to ensure energy conservation.

Associated materials databases include the electrical and thermal conductivities of the crucible and insulation material, the source and the boule material properties, the gas species and associated reactivity data, the induction frequency and the current density. The current database has been partially validated with external and indirect measurements. A precise knowledge of the thermophysical properties of the component materials of the reactor, as well as the powder, mono- and poly-crystal forms of SiC, are essential for obtaining realistic results [39, 40].

Multicomponent fluid transport. The fluid transport model is based on the low pressure kinetic theory of gases. Transport coefficients, such as viscosity, conductivity, specific heat, diffusivity and thermodiffusion coefficients, are calculated as local functions of temperature, pressure and composition. The Stefan–Maxwell formulation for diffusive transport ensures complete mass conservation of all species in the system. The transport database is interactive with the calculations and comes from the kinetic theory of gases.

For the modified Lely method with a graphite crucible, within the range of investigated experimental parameters, it was found that the natural convective transport of heat and of chemical species (buoyancy effects) can be neglected when compared to diffusive transport and heat conduction and radiation.

3.2. Selected results in heat and mass transfer

Overview. A generic representation of the different macroscopic fields is presented in figure 2. Magnetic vector potential contours for five turns of the coil and a frequency of 120 kHz are

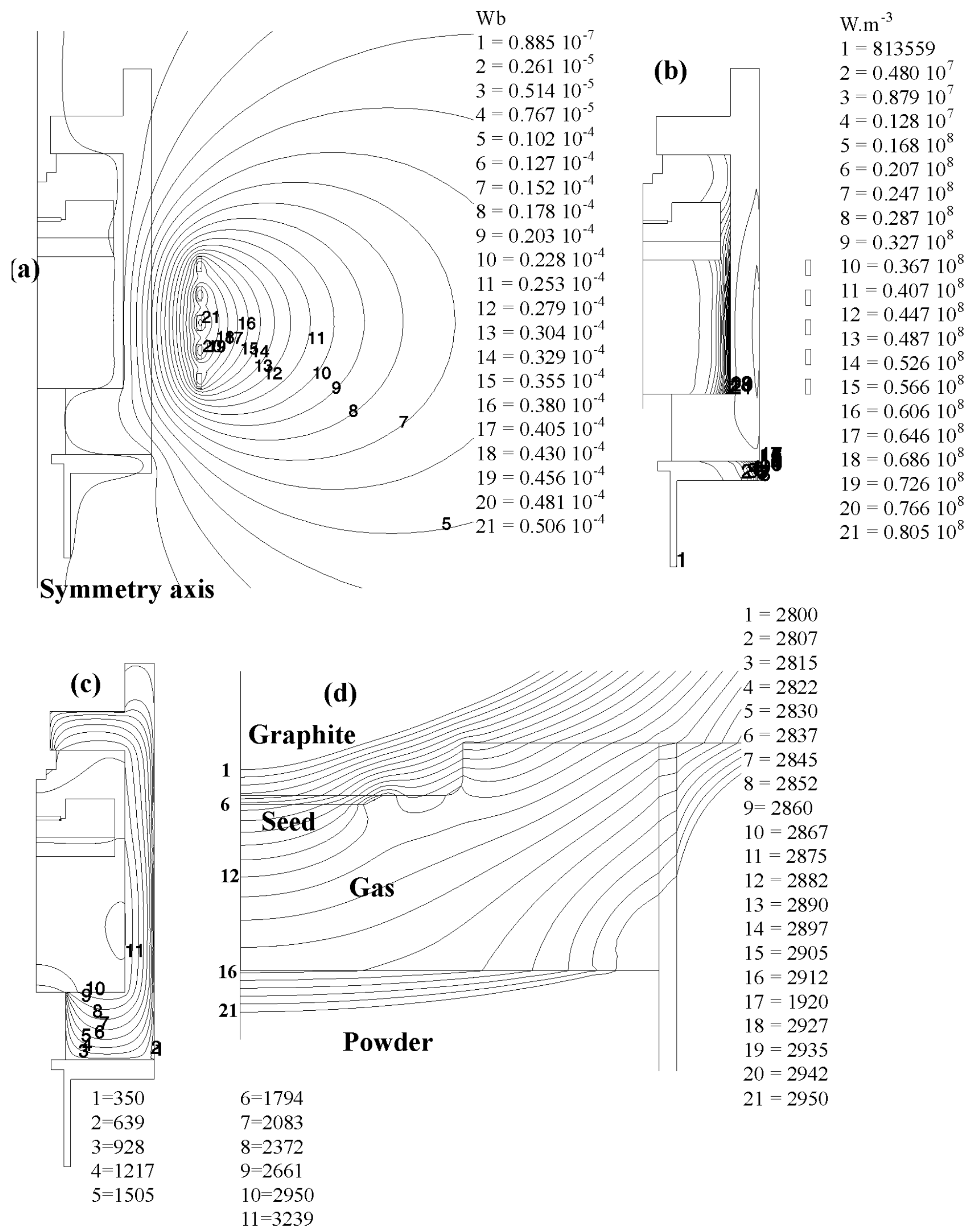

Figure 2. The right half of the axisymmetric reactor. (a) Potential vector, (b) Joule losses, (c) temperature field (K) (d) temperature field in the cavity ($f = 120$ kHz).

shown in figure 2(a). A large amount of energy is absorbed by the susceptor (figure 2(b)) within a thin skin depth. A temperature field is established inside the crucible (figure 2(c)). A thermal gradient of less than 80 K cm^{-1} is typical (see the enlargement in figure 2(d)).

Since the value of the growth rate is determined by the growth temperature, the total pressure in the system, the temperature difference between the surfaces of source and seed and

the seed–source distance. It is important to note, at this stage, that the challenge is to control small temperature differences (<100 K) in the gas cavity, as compared to the total temperature difference (about 2500 K).

This kind of simulation has been validated by changing frequency, current and coil position [27]. The numerical tool seems able to give guidelines for better control of the temperature field in the cavity.

Heat transfer: influence of the growing crystal. Many simulations have been performed at the beginning of the growth process. Nevertheless, it is also important to simulate the evolution of the temperature field as the growth proceeds. In fact, during the growth process, the distance between the crystal and the powder varies. The shape of the reaction chamber is modified and the variation of the electrical and thermal conductivities of the SiC powder due to its sintering and graphitization must be taken into account. An example of the evolution of the thermal field inside the reaction chamber as the crystal grows is given in figure 3. When the length of the boule increases, the radiative transfer inside the crucible leads to lower values of axial and radial temperature differences. The exact knowledge of this evolution is of importance for further discussions about the modelling of crystal shape, stress pattern, defect, dislocation and micropipe density.

Influence of the insulation. A graphite foam is always used around the crucible to ensure a good thermal insulation. Some experiments have been conducted with two different insulating foam thicknesses. The standard process with a large foam thickness leads to 4H polytype growth on 4H. Processes that have been carried out with a reduced foam thickness have led to crystals which initially grow with the 4H polytype and then switch to the 6H polytype (figure 4). Heat transfer simulation predicts a decrease of the radial temperature difference along the seed (30 mm in diameter) of about 30% when the thickness of the insulation is increased. It drops from 60 K, with poor insulation, to 40 K. These results indicate that a small increase of the radial temperature difference (in comparison with the working temperature) is sufficient to change the growth mode and strongly deteriorate the material.

Geometry modification and crystal shape. Some years ago, with seeds of 20 mm in diameter, two different configurations of the cavity were studied: a standard configuration (figure 5(a)) and a configuration with a flat screen acting as a radiation shield (figure 5(b)). The screen was used to prevent the formation of SiC deposits on the crucible around the seed. To provide this, a temperature field on the surface of the crucible, higher everywhere than the temperature of the surface of the growing crystal, should be established. This provides material transport predominantly to the seed. Mass transport modelling shows that no deposition occurs on the screen. The crystal grows with free boundaries. But, after an initial enlargement, the ingot diameter progressively decreases. The screen becomes too far from the growing interface to ensure the same conditions as in the first growth stages. This geometry allows the growth without poly-SiC but is inadequate to ensure a long-lasting enlargement due to changes in the thermal and flux fields during growth. Nowadays, the majority of reactors include advanced radiation shields to better control the growth and shape of the boule.

Influence of argon dilution. In addition to temperature, the partial pressures of argon and reactive species are among the process key parameters. It was simulated that for an argon pressure of 3 Torr (3.99 mbar), the crystal is convex (figure 6) and its shape more sensitive to the temperature field. When the argon pressure is increased to 7 Torr (9.3 mbar), i.e. the

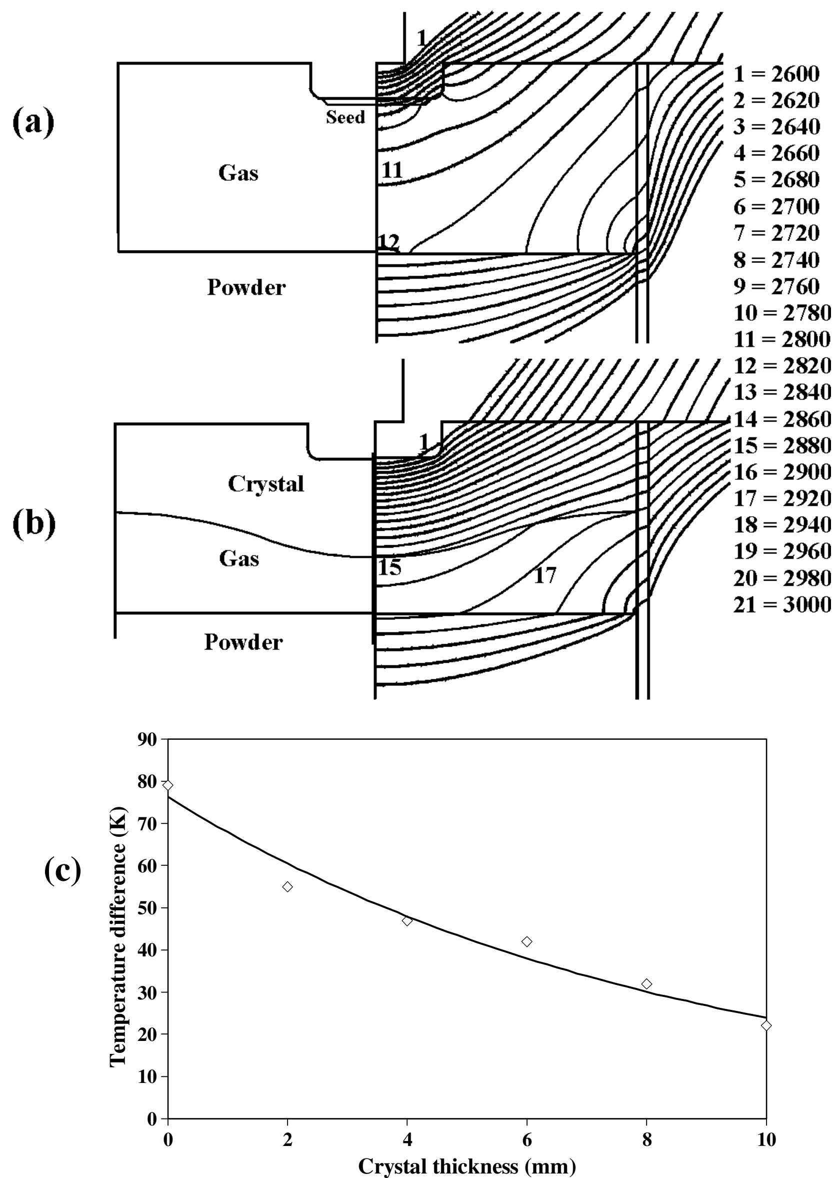

Figure 3. Influence of the crystal thickness on the thermal field and on the axial temperature difference in the cavity.

dilution of reactive species is increased, the growth rate decreases and the shape is less sensitive to the temperature field (the same for both cases at the beginning of the process). This example shows that it is possible to understand and quantify the final shape of the ingot. Generally, flat ingots are less likely to crack and a process less sensitive to variations of the temperature field is preferred.

These heat and mass transfer simulations may allow us to minimize design problems and complete the experimental and characterization approaches, but many technological problems, such as, for example, seed attachment, powder transformation, insulation ageing and quality, are not yet described by simulations.

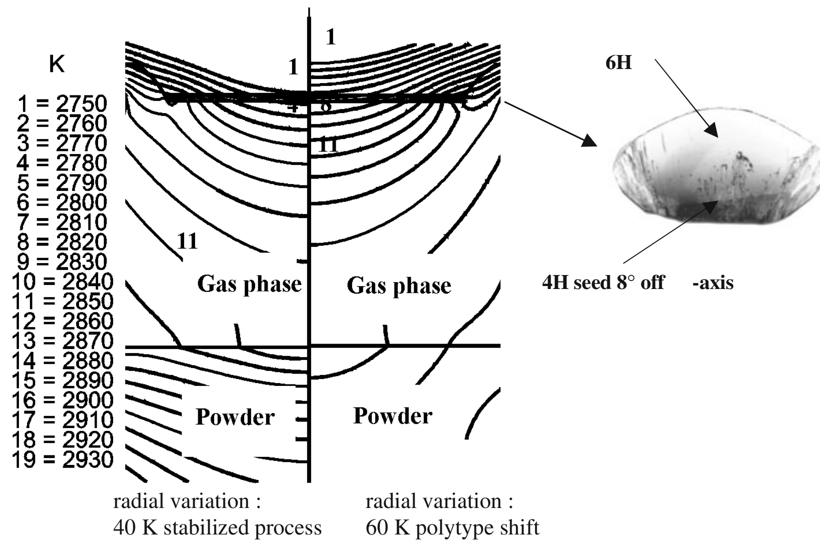

Figure 4. Influence of the foam thickness on heat transfer [33].

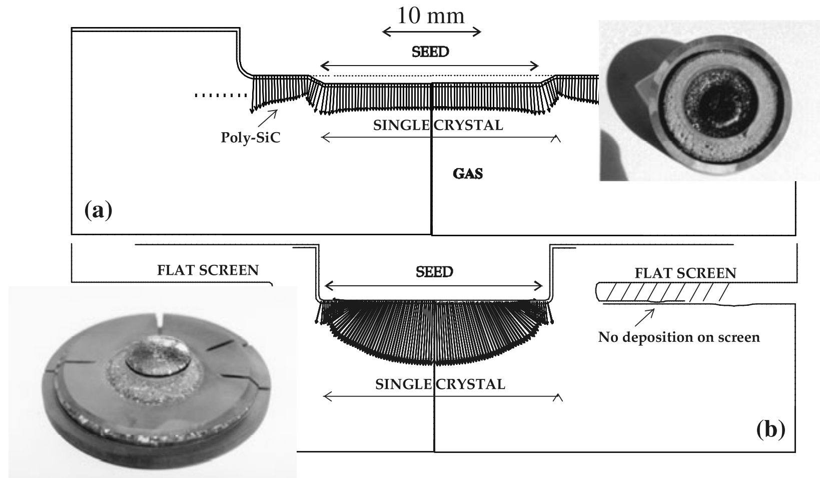

Figure 5. Initial growth flux for (a) a standard configuration and (b) a configuration with a flat screen inserted in the cavity.

Scaling-up of the reactor. With a heat transfer simulation, a design for the scaling-up of the previous reactor can be proposed, to keep similar temperature distributions. The pedestal supporting the seed is changed from 30 to 50 mm and all dimensions of the different parts of the reactor are increased. It is possible by changing frequency to obtain a temperature distribution in the cavity of the scaled-up reactor (right-hand side of figure 7) similar to that of the standard reactor (left-hand side of figure 7). This kind of quantification does not give all the keys to succeed but may allow us to minimize design problems.

Model development. The present development of the simulation tools is now focused on the prediction of dislocation formation [36, 41, 42]. Thermoelastic stresses are considered to be one of the reasons for the formation of crystalline defects (dislocations, micropipes). Not all

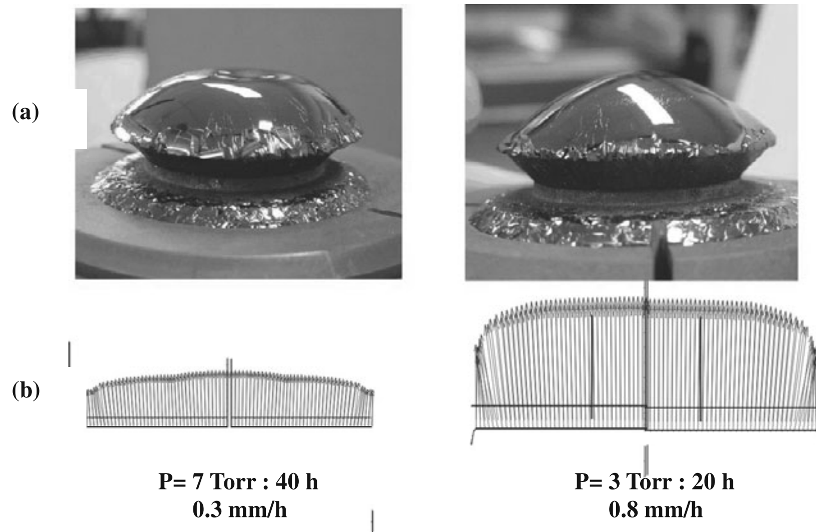

Figure 6. Influence of the argon pressure on the final shape of the crystal: (a) growth experiments, (b) simulation results of the reactive flux.

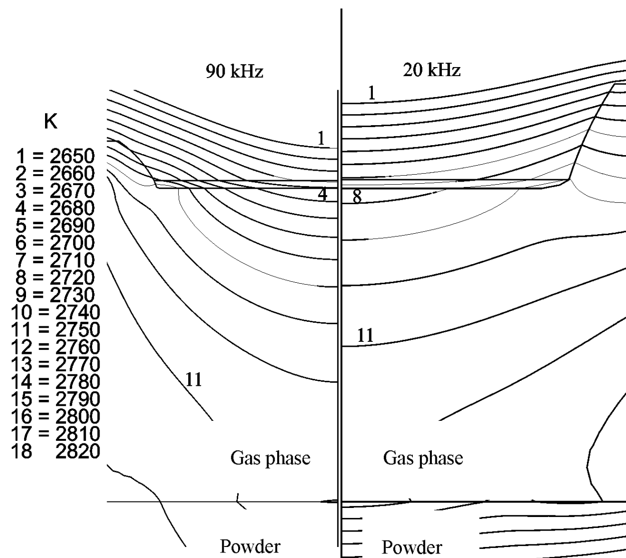

Figure 7. Influence of frequency heating on the scaling-up of the reactor.

thermoelasticity and plasticity [43] data are available to implement the model of dislocation generation and multiplication already used for silicon. Experiments and measurements analysis have to be conducted. However, with simple models, it was shown that the calculated stresses considerably exceed the critical resolved shear stress in SiC, which represents an indicator of the start of plastic deformation, i.e. formation of dislocations. This indicates that the observed dislocation network should be partly caused by thermal stresses. The thermoelastic approach can be used to correlate the temperature field in the growing crystal, its shape and the spatial distribution of dislocations.

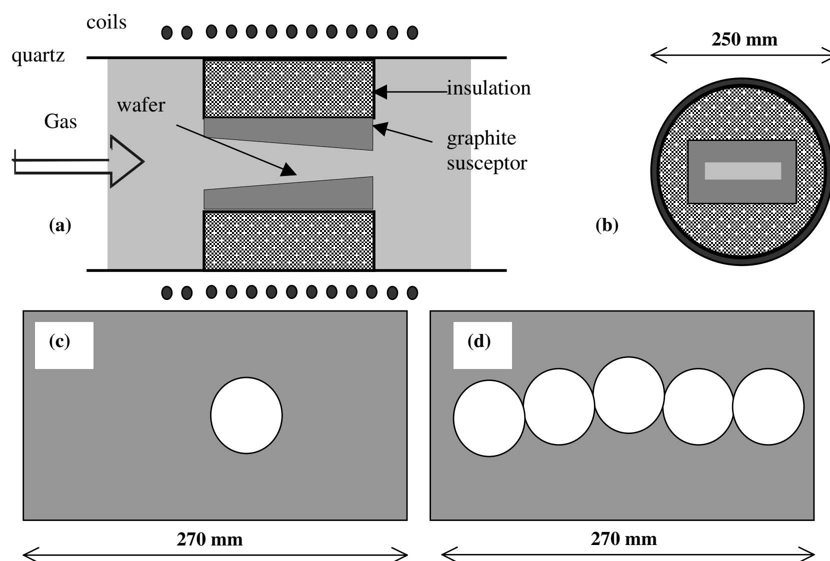

Figure 8. Schematic representation of the reactor: (a) plane view, (b) cross section, (c) standard position of a wafer of 2 inches on the graphite susceptor, (d) position of 5 wafers of 2 inches for specific experiments.

These first results show that careful control of the shape of the boule is needed to control the temperature gradient and the subsequent stress field.

4. Modelling and simulation of epitaxial growth

4.1. Introduction and specific needs

The experimental reactor from the Epigress Company (http://www.epigress.com) described elsewhere [16, 44] is schematically shown on figure 8. Silane and propane for SiC growth, nitrogen and TMA for doping, diluted in hydrogen, are used. The deposition pressure is fixed at 250 mbar and the temperature is in the 1700–1900 K range. The C/Si ratio in the gas phase is kept constant at 1. Deposition is made on the Si face of 4H SiC wafers. To visualize deposition, etching of SiC by H_2 and doping profiles along the susceptor, deposition and hydrogen etching runs have been carried out with 2 inch wafers placed at different locations on the graphite susceptor (figures 8(c) and (d)). The growth and etching rates are obtained via epilayer thickness measurements by infrared spectroscopy. Nitrogen and aluminium doping levels (n and p, respectively) are determined by C–V measurements with a Hg probe.

First, simulations involving electromagnetic, heat and mass transfer [12–16] were performed on this hot wall reactor to quantify the complex temperature distribution. The CFDACE software package (http://www.cfdrc.com) and a series of user subroutines was used. The rectangular shape of the susceptor, heated by induction, associated with the cylindrical shape of the insulation, leads to a 3D situation.

Second, mass transport simulations [12–16, 45] were performed to understand the history of growth rate and doping. The most complete and reliable heterogeneous and homogeneous kinetic database published was analysed [46–50], because numerous experiments support the validity of this database in the 1700–2000 K temperature range and 25–100 kPa pressure

Table 1. List of gas-phase and surface reactions included in the chemistry model. Etching reactions are shown in bold type (Si_s and C_s are surface sites).

Gas phase reactions	Surface reactions
$SiH_4 = SiH_2 + H_2$	$SiH_4 + C_s \rightarrow SiH_2_s + H_2 + C$
$Si_2H_6 = SiH_2 + SiH_4$	$\mathbf{C + Si_s + H_2 \rightarrow SiH_2 + C_s}$
$SiH_2 = Si + H_2$	$\mathbf{2Si + 2C_s + H_2 \rightarrow C_2H_2 + 2Si_s}$
$2H + H_2 = 2H_2$	$SiH_{2,s} \rightarrow H_2 + Si_s$
$C_3H_8 = CH_3 + C_2H5$	$SiH_2 + C_s \rightarrow SiH_{2,s} + C$
$CH_4 + H = CH_3 + H_2$	$Si + C_s \rightarrow Si_s + C$
$C_2H_5 + H = 2CH_3$	$C_2H_2 + Si_s \rightarrow 2C_s + H_2 + 2Si$
$2\ CH_3 = C_2H_6$	$C_2H_4 + Si_s \rightarrow 2C_s + 2H_2 + Si$
$C_2H_4 + H = C_2H_5$	$CH_4 + Si_s \rightarrow C_s + 2H_2 + Si$
$C_2H_4 = C_2H_2 + H_2$	$HSiCH_3 + C_s \rightarrow C + Si_s + H + CH_3$
$H_3SiCH_3 = HSiCH_3 + H_2$	$CH_3 + Si_s \rightarrow Si + C_s + 1.5H_2$
$H_3SiCH_3 = SiH_2 + CH_4$	$Si_2 + 2C_s \rightarrow 2C + 2Si_s$
$Si_2 = 2Si$	$Si_2C + Si_s \rightarrow Si_2 + Si + C_s$
$Si_2 + CH_4 = Si_2C + 2H_2$	$SiCH_2 + C_s \rightarrow C + Si_s + CH_2$
$SiH_2 + Si = Si_2 + H_2$	$CH_2 + Si_s \rightarrow C_s + Si + H_2$
$CH_3 + Si = SiCH_2 + H$	
$SiCH_2 + SiH_2 = Si_2C + 2H_2$	

range. The chemistry set finally adopted for the SiC deposition and etching is a simplified version of the models reported in the literature, completed with a few reactions containing H_3SiCH, H_3SiCH_3, $SiCH_2$ and Si_2C. It includes 18 gaseous species, 17 gas phase and 15 surface reactions listed in table 1. The surface reaction set is composed of chemical pathways which lead to SiC deposition and chemical pathways which lead to SiC etching (the ones that are indicated by bold type).

4.2. Experiments and simulation

4.2.1. Electromagnetic and heat transfer. The computations have been performed for standard conditions $P = 25$ kPa, $T_{max} = 1850$ K, $D_{H_2} = 80\ l\ min^{-1}$, a C/Si ratio of 1 and a high dilution for precursors (from 1 to 6×10^{-4} in mole). Due to the 3D shape of the susceptor and the position of the coil, the joule losses generated by the electromagnetic field are higher in the lateral parts and, consequently, the temperature is higher (figure 9). In addition, at the gas entrance of the susceptor, a cold finger contributes to this non-uniformity (figure 10). The temperature distribution along the susceptor varies from 1300 K at the entrance to 1750 K in the central part (figure 11). It is possible to modify it by increasing the thickness of the graphite (from 35 to 50 mm) and by changing the position and design of the coil [44]. Increasing the length of the graphite insulation [14] or of the coil is also a good way to improve the homogeneity of the temperature (figure 11). Work is in progress to find a good compromise between the technological constraints and the optimization of the temperature field. The 'best' temperature field is the one which gives the most uniform deposition and doping profiles over the largest dimensions. Consequently, the next step is to iteratively combine this 3D simulation with mass transfer and reactivity.

4.2.2. Mass transport and reactivity. In figure 12, the profiles of hydrogen etching rate and growth rate along the symmetry axis of the susceptor are shown for typical growth conditions (C/Si ratio = 1, high hydrogen dilution, $P = 250$ mbar, $T_{max} = 1850$ K). The

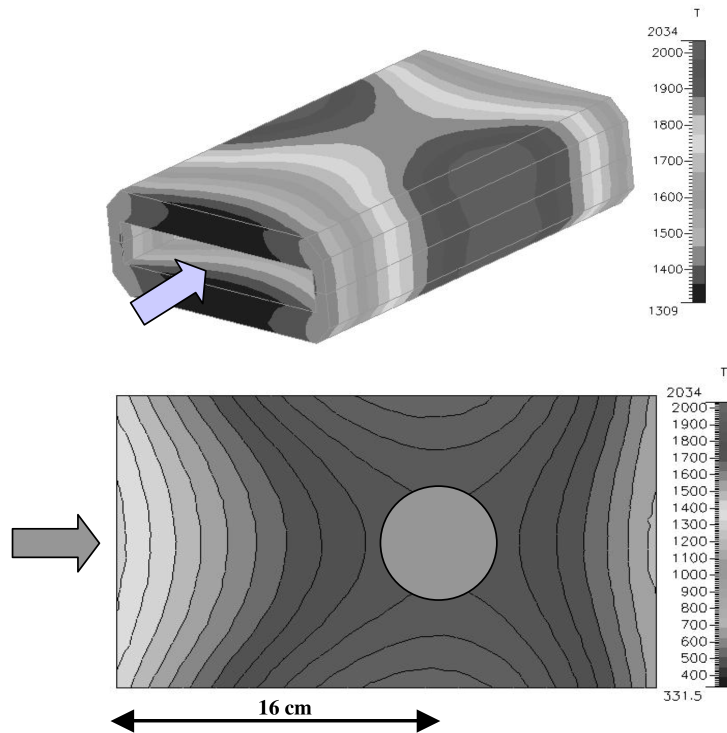

Figure 9. Temperature distribution (a) on the outside of the susceptor and (b) on the bottom of the susceptor; the 2 inch wafer is in its standard position.

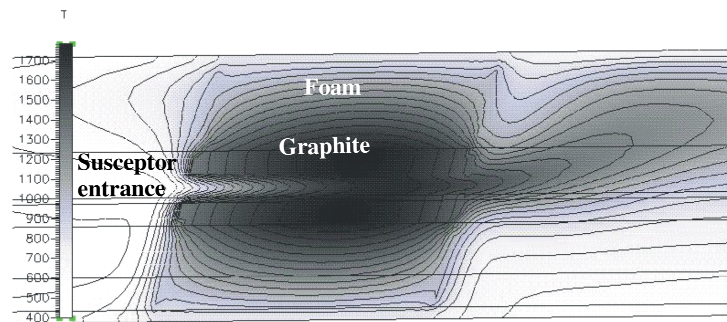

Figure 10. Influence of gravity and the narrow entrance of the susceptor on the temperature field ($P = 25$ kPa, $T_{max} = 1850$ K, $D_{H2} = 80$ l min^{-1}, C/Si ratio = 1 and 2×10^{-4} mole of SiH_4).

etching rate of the SiC surface increases to a maximum value of 0.6 μm h^{-1} in the first part of the susceptor. In the second part, it decreases, as temperature decreases, and deposition occurs from the species produced by the etching. Simulated results are in good agreement with the experimental values. In figure 12(b) are shown measured and simulated growth rates along the symmetry axis of the susceptor (with and without the etching model). There is good agreement between experimental and simulation results when gas and surface chemistry include etching phenomena during the growth process. With susceptor etching and the resulting production of gaseous species, it is possible to explain the uniform values of growth rate for the wafers located at a distance between 100 and 200 mm along the susceptor.

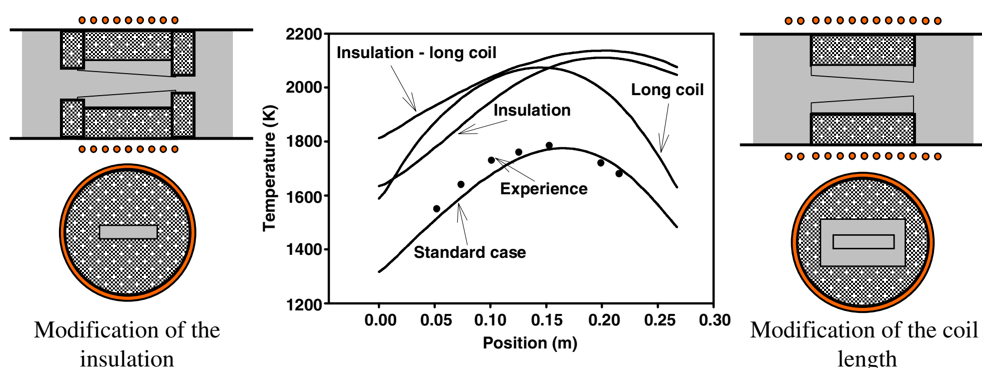

Figure 11. Temperature profile along the symmetry axis of the susceptor for different configurations.

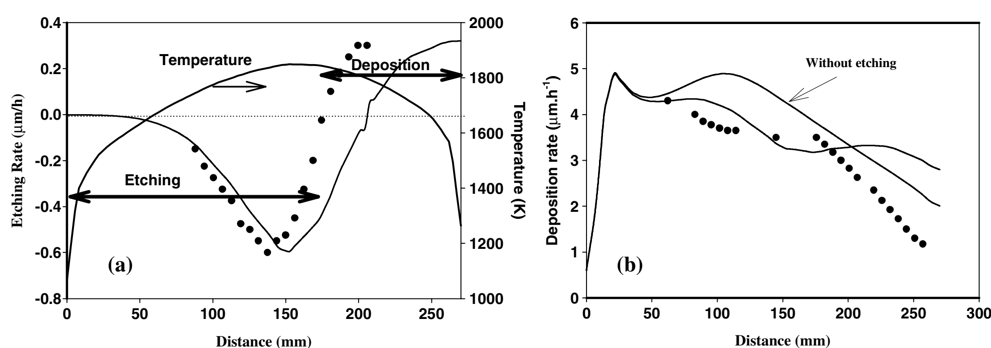

Figure 12. (a) Measured (●) and predicted (——) etching rates along the symmetry axis. Calculated temperature (broken line). (b) Measured (●) and predicted (——) growth rates along the symmetry axis of the susceptor.

Figure 13 shows the evolution of the experimental and simulated growth rate as a function of silane flow rate, in the centre of the middle wafer, while keeping the C/Si ratio constant at 1 in the gas phase. There is good agreement between simulation and experiment up to a given silane flow rate (20 sccm). At high precursor concentrations, the difference can be explained by secondary phase formation (i.e. silicon gas-phase condensation) [51] or parasitic deposition on the reactor walls.

This model predicts correctly the SiC deposition variations. SiC etching by hydrogen has a non-negligible impact during growth. The uniform deposition rate observed in the intermediate wafers results from the addition of precursors and the contribution of etching products. This also suggests the impact of susceptors on growth (unwanted dopants, etc) and might be an interesting starting point to begin a modelling study of doping.

The nitrogen and aluminium doping levels (n and p, respectively) measured along the susceptor are shown in figure 14.

For the development of a doping model, we first attempted to find a correlation between experimental doping results and the major growth parameters, i.e. temperature and growth rate. Figure 15 shows distributions of doping level (for p doping), growth rate and calculated temperature in the middle of the reactor (130–170 mm). There is no direct correlation between doping and growth rate distributions. However, similar trends are found between doping and temperature distributions (figures 15(a) and (c)). Doping increases with decreasing

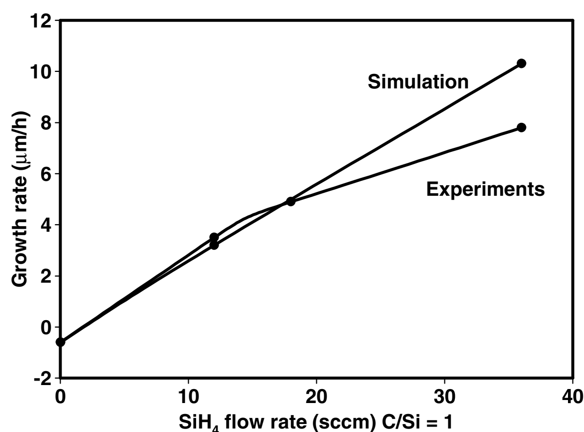

Figure 13. Evolution of the calculated and experimental growth rates versus silane flow rate, keeping constant the C/Si ratio (=1) in the gas phase and the hydrogen flow rate.

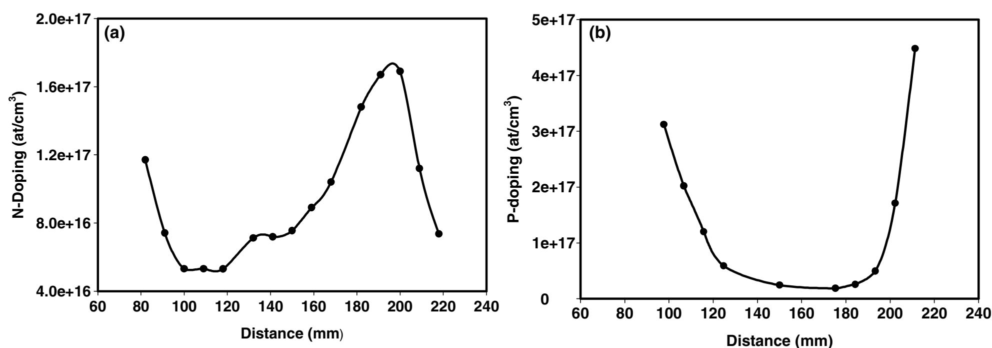

Figure 14. Experimental evolution of n-doping (a) and p-doping (b) versus distance along the susceptor for typical growth conditions.

temperature. It has been found that increasing the temperature by 250 °C leads to a decrease in doping by one order of magnitude. That suggests that doping is slightly temperature-activated. However, it can be concluded that doping level is the result of various intricate phenomena.

Thermodynamic analyses have been carried out to identify the potential and important gaseous species (see also [51]). Figure 16 indicates the major species present at equilibrium in the Si–C–N–H (a) and Si–C–Al–H (b) systems as a function of temperature for the given pressure of 250 mbar.

For the Si–C–N–H system, it is found that the gas-phase reactions producing the radicals HCN and SiNH are relatively slow. Since the residence time in the hot zone is very short, it is not likely that these species contribute significantly to surface reactivity mechanisms even though they should be very reactive. Therefore, the precursor N_2 might be the main contributing species to the nitrogen incorporation, even though its reactivity is low. In order to represent the differences found between doping incorporation versus surface polarity and the well-known site competition [52], we add to the previously presented Si–C model [53] a simple model where nitrogen replaces carbon, with a very low sticking coefficient. The obtained n-doping results along the susceptor are given in figure 17. The correct value is obtained in the middle of the susceptor. However, even though the evolution versus distance

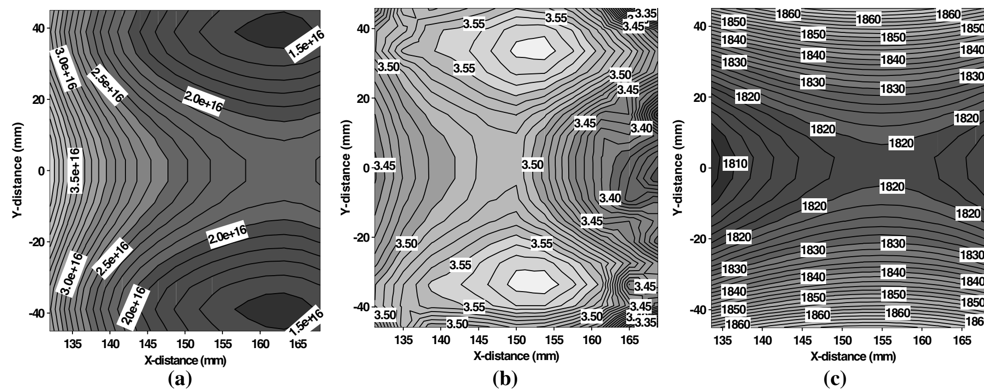

Figure 15. Distributions of (a) doping level (for p doping), (b) growth rate and (c) calculated temperature in the middle part of the susceptor for typical growth conditions.

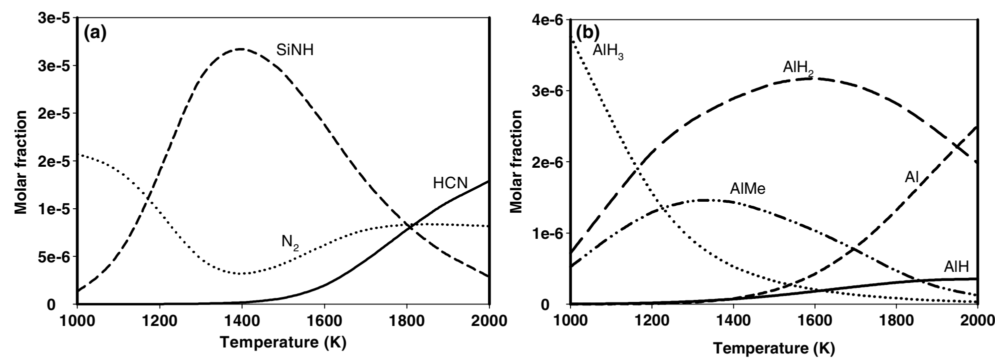

Figure 16. Homogeneous thermodynamic calculations in the Si–C–N–H (a) and Si–C–Al–H (b) systems at a pressure of 250 mbar.

is similar to the experimental behaviour (i.e. doping increases), the variations are not large enough. That suggests that other mechanisms, such as nitrogen desorption (which is highly temperature-dependent), should be included to correctly describe the nitrogen incorporation. Work is continuing to produce more complete models.

5. Conclusions

The examples of SiC single crystals and thin films illustrate how modelling and simulation play a significant role in improving the current knowledge and in helping engineers in the design and optimization of the process equipment. It is not yet possible to build a single model that captures all the involved physics and chemistry of silicon carbide growth processes and covers all time and length scales. The macroscopic approach linked with experiments and characterization allows us to open, step by step, the black box of the process and to gain an insight into the intricate mixture of phenomena. The characterization and simulation results are complementary to understanding the growth mechanisms, and consequently the structural quality, defect formation and deposition profile. Some relationships between all these information and operating parameters were proposed.

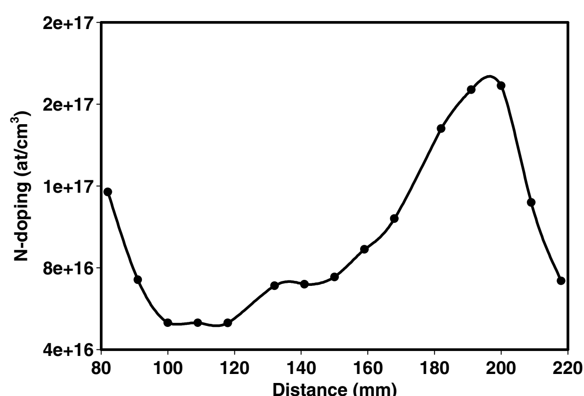

Figure 17. Simulated N-doping along the susceptor.

Acknowledgments

The authors gratefully acknowledge the long term support of the French Ministry of Education and Research, the 'Région Rhônes-Alpes', ST Microelectronics and the 'Alternative SiC' network. Most of the work was carried out under the Brite-Euram 'JESICA' project.

References

[1] Cooper J A 2002 *Mater. Sci. Forum* **289–393** 15
[2] Di Cioccio L and Billon T 2002 *Mater. Sci. Forum* **289–393** 1119
[3] Müller St G, Brady M F, Brixius W H, Fechko G, Glass R C, Henshall D, Hobgood H McD, Jenny J R, Leonard R, Malta D, Powell A, Tsvetkov V F, Allen S, Palmour J and Carter C H Jr 2002 *Mater. Sci. Forum* **289–393** 23
[4] Matsunami H 2002 *Mater. Sci. Forum* **289–393** 3
[5] Bergman J P, Jakobsson H, Storasta L, Carlsson F H C, Magnusson B, Sridhara S, Pozina G, Lendenmann H and Janzen E 2002 *Mater. Sci. Forum* **289–393** 9
[6] Ellison A, Zhang J, Magnusson W, Henry A, Wahab Q, Bergman J P, Hemmingson C, Son N T and Janzen E 2000 *Mater. Sci. Forum* **338–342** 1312
[7] Neyret E 2000 *PhD Thesis* Institut National Polytechnique de Grenoble, France
[8] Rupp R, Makarov Yu N, Behner H and Wiedenhofer A 1997 *Phys. Status Solidi* b **202** 281
[9] Vorob'ev A N, Komissarov A E, Segal A S, Makarov Yu N, Karpov S Yu, Zhmakin A I and Rupp R 1999 *Mater. Sci. Eng.* B **61/62** 76
[10] Vorob'ev A N, Egorov Yu E, Makarov Yu N, Zhmakin A I, Galyukov A O and Rupp R 1999 *Mater. Sci. Eng.* B **61/62** 172
[11] Hasegawa M, Miyauchi A, Masahara K, Ishida Y, Kakahashi T, Ohno T, Nishio J, Suzuki T, Tanaka T, Yoshida S and Arai K 2002 *Mater. Sci. Forum* **289–393** 227
[12] Lofgren P M, Hallen C, Gu C Y and Ji W 2000 *Mater. Sci. Forum* **338–342** 153
[13] Lofgren P M, Ji W, Hallen C and Gu C Y 2000 *J. Electrochem. Soc.* **147** 164
[14] Danielsson Ö, Henry A and Janzen E 2002 *J. Cryst. Growth* **243** 170
[15] Danielsson Ö, Fosberg U, Henry A and Janzen E 2002 *J. Cryst. Growth* **235** 352
[16] Pons M, Meziere J, Tang Kuan S W, Blanquet E, Ferret P, Di Cioccio L, Billon T and Madar R 2002 *Mater. Sci. Forum* **289–393** 223
[17] Wischmeyer F, Kappeler J, Berge R, Fornell J, Dauelsberg M, Heuken M and Jurgensen H 2001 *Mater. Sci. Forum* **353–356** 103
[18] Kimoto T, Nakazawa S, Fujihira K, Hirao T, Nakamura S, Chen Y, Hashimoto K and Matsunami H 2002 *Mater. Sci. Forum* **289–393** 165
[19] Mashara K, Takahashi T, Kushibe M, Ohno T, Nishio J, Kojima K, Ishida Y, Suzuki T, Tanaka T, Yoshida S and Arai K 2002 *Mater. Sci. Forum* **289–393** 179

[20] Moulin C, Pons M, Pisch A, Grosse P, Faure C, Basset G, Passero A, Billon T, Pelissier B, Anikin M, Pernot P and Madar R 2001 *Mater. Sci. Forum* **353–356** 7
[21] Pernot E, Neyret E, Moulin C, Pernot-Rejmankova P, Templier F, Di Cioccio L, Billon T and Madar R 2002 *Mater. Sci. Forum* **289–393** 419
[22] Vincente P, Pernot E, Chaussende D and Camassel J 2002 *Mater. Sci. Forum* **289–393** 729
[23] Hofmann D, Heinze M, Winnaker A, Durst F, Kadinski L, Kaufmann P, Makarov Yu N and Schäfer M 1995 *J. Cryst. Growth* **146** 214
[24] Pons M, Blanquet E, Dedulle J M, Garcon I, Madar R and Bernard C 1996 *J. Electrochem. Soc.* **143** 3727
[25] Pons M, Anikin M, Dedulle J M, Madar R, Chourou K, Blanquet E and Bernard C 1997 *Surf. Coat. Technol.* **94/95** 279
[26] Karpov S Yu, Makarov Yu N and Ramm M S 1997 *Phys. Status Solidi* b **202** 201
[27] Pons M, Anikin M, Chourou K, Dedulle J M, Madar R, Blanquet E, Pisch A, Bernard C, Grosse P, Faure C, Basset G and Grange Y 1999 *Mater. Sci. Eng.* B **30** 18
[28] Klein O, Philip P, Sprekels J and Wilmanski K 2001 *J. Cryst. Growth* **222** 832
[29] Nishisawa S, Kato T, Oyanagi N and Arai K 2002 *Mater. Sci. Forum* **389–393** 43
[30] Ma R H, Chen Q S, Zhang H, Prasad V, Balkas C M and Yushin N K 2000 *J. Cryst. Growth* **211** 352
[31] Selder M, Kadinski L, Makarov Y, Durst F, Wellmann P, Straubinger T, Hofmann D, Karpov S and Ramm M 2000 *J. Cryst. Growth* **211** 333
[32] Yakimova R, Syvajarvi M, Dedulle J M, Pons M and Janzen E 2001 *Proc. 1st Int. Conf. on Microgravity Research and Applications in Physical Sciences and Biotechnol (SP-454)* vol 1 (Noordwijk: ESA) p 381
[33] Moulin C, Pons M, Pisch A, Grosse P, Faure C, Basset A, Basset G, Passero A, Billon T, Pelissier B, Anikin M, Pernot E, Pernot Rejmankova P and Madar R 2001 *Mater. Sci. Forum* **353–356** 7
[34] Bogdanov M V, Galyukov A O, Karpov S Yu, Kulik A V, Kochuguev S K, Ofengeim D, Tsiryulnikov A V, Ramm M S, Zhmakin A I and Makarov Yu N 2001 *J. Cryst. Growth* **225** 307
[35] Chen Q S, Zhang H and Prasad V 2001 *J. Cryst. Growth* **230** 239
[36] Pons M, Moulin C, Dedulle J M, Pisch A, Pelissier B, Blanquet E, Anikin M, Pernot E, Madar R, Bernard C, Faure C, Billon T and Feuillet G 2001 *Mater. Res. Soc. Symp. Proc.* **640** H1.4
[37] Pisch A, Blanquet E, Pons M, Bernard C, Anikin M, Dedulle J M and Madar R 1999 *J. Physique* IV **9** 213
[38] Pisch A, Ferraria A M, Chatillon C, Blanquet E, Pons M, Bernard C, Anikin M and Madar R 2000 *Mater. Sci. Forum* **338–342** 91
[39] Muller St G, Fricke J, Hofmann D, Horn R, Nilsson O and Rexer B 2000 *Mater. Sci. Forum* **338–342** 43
[40] Muller St G, Eckstein R, Fricke J, Hofmann D, Hofmann R, Horn R, Mehling H and Nilsson O 1998 *Mater. Sci. Forum* **264–268** 623
[41] Zhmakin I A, Kulik A V, Karpov S Y, Demina S E, Ramm M S and Makarov Yu N 2000 *Diamond Relat. Mater.* **9** 446
[42] Selder M, Kadinski L, Durst F and Hofmann D 2001 *J. Cryst. Growth* **226** 501
[43] Karpov S Yu, Kulik A V, Ramm M S and Makarov Yu N 2003 *Mater. Sci. Forum* at press
[44] Pons M, Mézière J, Wan Tang Kuan S, Dedulle J M, Blanquet E, Di Cioccio L, Ferret P and Billon T 2001 *J. Physique* IV **11** 1079
[45] Vorob'ev A N, Karpov S Yu, Bogdanov M V, Komissarov A E, Bord O V, Zhmakin A I and Makarov Yu N 2002 *Comput. Mater. Sci.* **24** 520
[46] Allendorf M D and Melius C 1992 *Phys. Chem.* **96** 428
[47] Allendorf M D and Melius C 1993 *Phys. Chem.* **97** 720
[48] Aubreton J, Blanquet E, Echlinger M F and Pons M 1998 *Ann. Chim., Sci. Mater.* **23** 75
[49] Allendorf M D and Kee R J 1991 *J. Electrochem. Soc.* **138** 841
[50] Raffy C, Blanquet E, Pons M, Bernard C, Melius C F and Allendorf M D 1999 *J. Physique* IV **9** 205
[51] Forsberf U, Danielsson Ö, Henry A, Linnarsson M K and Janzen E 2002 *J. Cryst. Growth* **236** 101
[52] Larkin D J, Neudeck P G, Powell J A and Matus L G 1994 *Appl. Phys. Lett.* **65** 1659
[53] Danielsson Ö, Forsberg U and Janzen E 2003 *J. Cryst. Growth* at press